RESEARCH ARTICLE

Empirical equations for flexural residual strengths in concrete with low volumetric fractions of hook-end steel fiber

Aaron Kadima Lukanu Lwa Nzambi | **Jeandry Bule Ntuku** |
Dênio Ramam Carvalho de Oliveira

Civil Engineering School, Federal
University of Pará, Belém, Brazil

Correspondence
Aaron Kadima Lukanu Lwa Nzambi, Civil
Engineering School, Federal University of
Pará, Belém, Pará, Brazil.
Email: aaronkadima@gmail.com

Abstract

The characterization of steel fiber concrete in a flexural test or tensile uniaxial test requires greater control of loading rate by the speed applied in the test machine, to be able to report more accurately the behavior of displacements or crack openings in micro-scale possible. In general, in the pre-dimensioning process, it is often discarded the characterization tests and the main standards do not provide theoretical design recommendations concerning the residual strengths of fibrous concrete. Some empirical models in the literature attempt an approximation of the theoretical design values, but they present greater dispersion in the results. This article proposes empirical equations for predicting the residual strengths of the steel fiber reinforced concrete (SFRC), for small fiber volume fractions (approx. < 0.8%). Experimentally notched beams subjected to three-point bending tests were collected, with the concrete matrix composed of hook-end steel fiber and the experimental residual strengths presenting the softening behavior in the load-opening ratio curve of the crack. The experimental residual strengths were compared with other empirical models found in the literature. The results showed that the maximum stress of the steel fiber pullout model established satisfactory relationships with the residual stresses in flexure. The empirical proposed residual strength model presented lower variability of dispersion around 10%, the mean absolute percentage error of 8%, compared to other usual empirical models and had the same material class with the experimental results, proving to be a viable alternative for pre-design and dosage optimization for SFRC.

KEYWORDS
adherence, notched beam, residual stress, steel fiber

JEL CLASSIFICATION
Civil and environmental engineering

1 | INTRODUCTION

The knowledge of the mechanical behavior of the materials used in civil construction is fundamental for the safe and economical designing of reinforced concrete (RC) structures. With the emergence of new materials, such as steel fibers reinforced concrete (SFRC), it is necessary to perform the characterization tests of these materials, to obtain an economical dosage and satisfactory mechanical properties of a cementitious matrix.

It is known that short steel fibers added in concrete as mass reinforcement mainly provide crack control due to the tensile stress transfer capability of the fibers across crack surfaces known as crack-bridging, after cracking. This way, fibers provide significant resistance to shear across developing cracks, and therefore, steel fibre reinforced concrete (SFRC) demonstrate a pseudo-ductile response,[1] increased residual strength (especially in tension) and enhanced energy dissipation capacities, relative to the brittle behavior of plain concrete mixtures. Further, the advantageous characteristics of SFRC under tension are also very important for the shear response of concrete structural members which is governing by the tensile response of the fibrous material. Thus, fibers have been proved as a promising non-conventional reinforcement[2,3] in concrete elements under shear stresses due to the beneficial cracking performance of SFRC and, under specific circumstances, could alter the brittle shear failures to ductile flexural ones.

According to Barros,[4] the properties of concrete most benefited by steel fiber reinforcement mechanisms are the energy absorption capacity, ductility, cracking control and improved toughness. As for the application, highlights include its use in industrial floors, road and airport sidewalks, tunnel linings, anchorage blocks for prestressing cables or in other regions with stress concentration, in precast in general, and the reinforcement of structural elements.[5]

After the SFRC cracks open, the load is transferred immediately to the fibers at the crack interface. Due to fiber debonding, the load tensile stress response drops abruptly and is stopped at a certain level by the fiber pull-out strength, generating a bridging effect.[6] The stress at this level is defined as the post-cracking strength. According to CEB-FIP and ACI 544.4R-88,[7] the post-cracking behavior of the load–displacement curve can provide softening response (single crack)[5] or hardening (when multiple cracks are formed before the concrete reaches the maximum tensile load). These responses depend on the composition of the SFRC, such as the type and amount of fiber. For softening behavior material, typical of a uniaxial test, the maximum strength, may be assumed equal to the maximum stress and the residual uniaxial tensile strength of the material, is significantly affected by the volume fraction of fibers (V_f), by the aspect ratio (l_f/d_f), as well as the bond between concrete and steel, therefore the execution of this test is not simple, it is not appropriate to represent the standard test for new mixtures, because of the complexity of interpreting the results.

Thus, CEB-FIP[8] and RILEM TC 162-TDF[9] report that bending test may be performed to establish the tensile behavior of the SFRC. The aforementioned standards suggest the three-point (3 PB) bending test on notched beams, but the divergences in the performing of these tests and the interpretation of the results generate even more complexity in the attempts to have a theoretical model that adequately simulates the behavior of the material when the results of proper characterization tests are not available. According to Parmentier and De Grove,[10] the results provided by the bending test suggested in the RILEM TC 162-TDF[9] have a coefficient of variation between 10% and 25% (results obtained in specimens with 30 kg/m³ of steel fiber).

In fib Model Code[8] the post-cracking behavior is influenced by the characteristic values of residual flexural tensile strengths (f_{Ri}) calculated as a function of the crack opening, crack mouth opening displacement (CMOD) or load–displacement constitutive relationship. There is no consensus in the literature for analytical models development. There are studies[11,12,13] that use the linear regressions generated from the basic properties of the composite materials, as the compressive strength of the concrete matrix and the product of the fiber content by the fiber aspect ratio, the fiber reinforcement index (RI), to predict the residual flexural strength of SFRC. Therefore, these regressions do not always provide the results that converge satisfactorily for several reasons, considering the variabilities of the parameters such as the type of concrete compactness,[11,14] the type of fiber shape, and the sensitivity of the test method used. Thus, theoretical predictions are subject to considerable variability. According to Moraes-Neto et al.[12] a relatively large scatter of results is naturally expected (CV = 27%–36%), whereas, Venkateshwaran et al. observed a coefficient of variation around 25%. Table 1 presents the summary of the empirical approach of residual strengths proposed by Moraes-Neto et al.[12] and by Venkateshwaran et al.[13]

This work proposes a new empirical model for predicting the residual strengths for the design procedure with fib Model Code,[8] In concrete with low steel fiber content, high rates can either weaken the workability[5,15] in the fresh state or considerably influence the mechanical property responses of the SFRC hardened state. The equations include the most significant parameters governing the tensile behavior of SFRC, tensile stress at failure pull-out and fiber content. Parameters as inclination,[16,17] the number of hooked ends,[18,13,19] and random distribution[1] of steel fibers were not considered.

TABLE 1 Empirical equations for characteristic residual flexural strengths

f_{Ri}	Empirical approach	
	Moraes-Neto et al.[12]	Venkateshwaran et al.[13]
$f_{R1,d}$	$7.5 \cdot (RI)^{0.8}$	$\Psi \cdot \left[0.320 \cdot (f_c)^{0.5} + 6.214 \cdot (RI) + 0.034 \cdot N^2\right]$
$f_{R2,d}$	-	$\Psi \cdot \left[0.353 \cdot (f_c)^{0.5} + 7.337 \cdot (RI) + 0.300 \cdot N^2\right]$
$f_{R3,d}$	$6.0 \cdot (RI)^{0.7}$	$\Psi \cdot \left[0.300 \cdot (f_c)^{0.5} + 7.629 \cdot (RI) + 0.373 \cdot N^2\right]$
$f_{R4,d}$	$5.5 \cdot (RI)^{0.65}$	$\Psi \cdot \left[0.284 \cdot (f_c)^{0.5} + 7.018 \cdot (RI) + 0.343 \cdot N^2\right]$

Note: RI is the fiber reinforcement index, $V_f \cdot \left(l_f/d_f\right)$; factor Ψ is a factor which takes into account the fiber length, $\Psi = \left(1 + l_f/100\right)^{0.5}$; and N is the number of the hook-ends in steel fiber.

To further prove the model's effectiveness, a comparison with the other models found in the literature and described above is also reported at the end of the article.

2 | MODEL CODE 10 RECOMMENDATIONS AND DESIGN METHODS

Figure 1 shows the process of performing three-point bending tests (3PBT) according to Model Code10.[8] It is recommended that the equipment responsible for reading the notch opening (CMOD reading) be installed in the center of the beam and along its longitudinal axis. The reference distance for the CMOD measurement should not be greater than 40 mm and the distance between the bottom of the beam and the equipment axis should be less than 5 mm. The accuracy of the CMOD should be 0.01 mm and the accuracy of the equipment used in reading the loading should be 0.1 kN. The loading rate must be controlled. The Model Code10 [8] provides four residual strengths, $f_{R1}, f_{R2}, f_{R3},$ and f_{R4}, which correspond respectively to CMOD of 0.5, 1.5, 2.5, and 3.5 mm. The residual strengths are calculated according to Equation (1).

$$f_{Ri} = \frac{3 \cdot F_{R,i} \cdot L}{2 \cdot b \cdot h_{sp}^2} \tag{1}$$

where, $F_{R,i}$ refers to the load registered in $CMOD_i$; L, b, and h_{sp} are the geometry measurements of the notched prism.

2.1 | Tensile stress at pull-out failure

The maximum fiber tensile stress ($\sigma_{f,max}$) can be obtained by dividing the maximum pull-out load (F_{max}) per the nominal cross-sectional area of the fiber (A_f), Equation (2). According to Nzambi et al.[5] the maximum pull-out load of SFRC can be calculate by Equation (3). Where, λ, e, φ are parameters that take into account the influence of fiber volume on fiber adherence length and f_{ct} is tensile strength in flexural and defined as $0.3 \cdot f_c^{2/3}$.

$$\sigma_{f,max} = \frac{F_{max}}{A_f} \tag{2}$$

$$F_{max} = \lambda \cdot \pi \cdot d_f \cdot l_f^{\varphi} \cdot f_{ct} \tag{3}$$
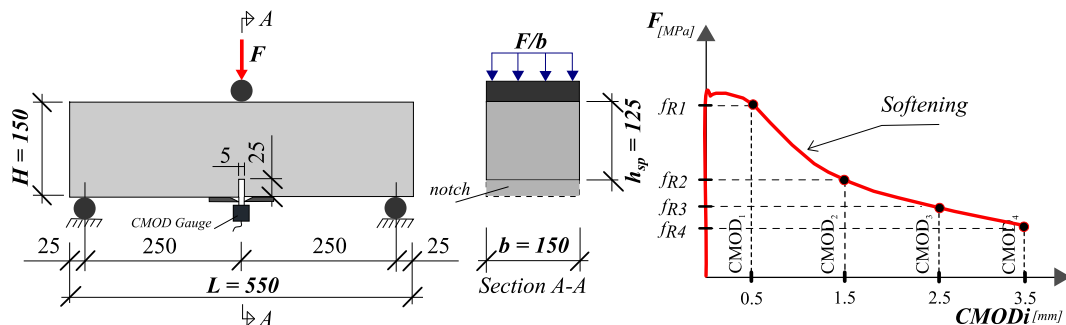

FIGURE 1 3P prism notched test (mm) and f_{Ri} x CMODi diagram (Model Code[5])

where, d_f is the fiber diameter and l_f is the embedment length of steel fiber. The maximum tensile stress induced in the fiber ($\sigma_{f,\max}$) can be calculated using Equation (4), substituting Equation (2) into (1).

$$\sigma_{f,\max} = 4 \cdot \lambda \cdot f_{\mathrm{ct}} \cdot \left(\frac{l_f^{\varphi}}{d_f}\right) > \sigma_{fy} \tag{4}$$

According to Dancygier and Savir,[20] the tensile stress, resisted by fibers bridging a unit area of the inclined crack is calculated from Equation (5). The fiber bond strength, τ_f is taken as 4.15 MPa.

$$\sigma_f = 2 \cdot \tau_f \cdot \left(\frac{l_f}{d_f}\right) \leq \sigma_{fy} \tag{5}$$

2.2 | Strain constitutive law

Tensile stress versus strain constitutive law of SFRC greatly influence the flexural response of the prismatic notched specimens, the uniaxial first crack tensile strength of fiber reinforced concrete, f_{Ft}, may be assumed equal to that of the matrix, f_{ct}.[21,22] For softening behavior material, the strength, f_{Ft}, may be assumed equal to the maximum stress (Figure 2A). The simplified constitutive laws for representing the tensile behavior of SFRC, according to Model Code,[8] are shown in Figure 2B. The stress-crack opening relationship in uniaxial tensile characterizes the post-cracking behavior of the material, in linear elastic model or a rigid-plastic model, where f_{Fts} and f_{Ftu}, concerning serviceability limit state (SLS) and ultimate limit state (ULS) behavior respectively. According to Model Code,[8] the f_{R1} strength values indicate the material classes in flexure, ranging from 1 to 8 MPa. Whereas the f_{R3}/f_{R1} ratio is denoted by the letters a, b, c, d, e, corresponds to the classification presented in Table 2, softening or hardening materials.

2.3 | Database (DB) details

The DB used in the analysis is formed by 13 different works reported by the literature, consisting of 46 experimental flexural tests at three points of notched prisms, as defined in Reference 8, see Table 3. These beams were reinforced only
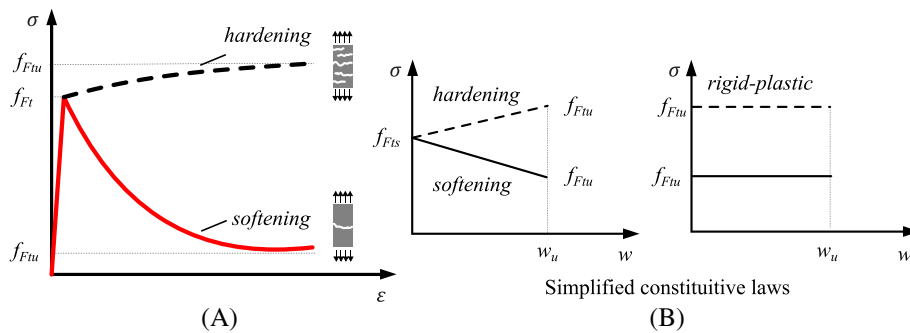

FIGURE 2 Tensile behavior of SFRC: (A) Tensile stress versus strain. (B) Simplified constitutive laws

TABLE 2 Classification according to Model Code[8]

Class	f_{R3}/f_{R1}	Behavior
a	0.5	Softening
b	0.7	
c	0.9	
d	1.1	Hardening
e	1.3	

TABLE 3 Beams residual strength database

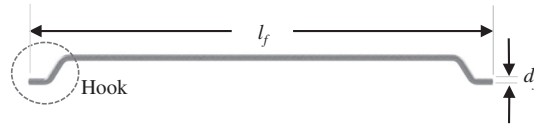| Id. | f_c (MPa) | V_f (%) | l_f (mm) | d_f (mm) | l_f/d_f | Experimental $f_{Ri,EXP}$ | | | |
						f_{R1} (MPa)	f_{R2} (MPa)	f_{R3} (MPa)	f_{R4} (MPa)
AM-0.4-EH1[23]	61.30	0.40	35.00	0.55	63.64	4.99	4.11	3.32	2.73
AM-0.8-EH1[23]	63.80	0.80	35.00	0.55	63.64	7.44	7.08	5.68	4.63
AM-0.4-EH2[23]	63.60	0.40	60.00	0.90	66.67	5.35	5.90	5.53	5.05
AM-0.8-EH2[23]	58.70	0.80	60.00	0.90	66.67	7.94	9.48	8.78	7.56
AM-0.4-EH1[24]	61.30	0.40	35.00	0.55	63.64	5.49	4.05	3.03	2.36
AM-0.4-EH1[24]	61.30	0.40	35.00	0.55	63.64	4.37	3.91	3.28	2.79
AM-0.4-EH1[24]	61.30	0.40	35.00	0.55	63.64	4.67	3.49	2.98	2.37
AM-0.4-EH1[24]	61.30	0.40	35.00	0.55	63.64	5.22	3.92	3.06	2.58
AM-0.4-EH1[24]	61.30	0.40	35.00	0.55	63.64	4.74	4.16	3.50	2.88
AM-0.4-EH1[24]	61.30	0.40	35.00	0.55	63.64	5.46	5.14	4.09	3.39
AM-0.4-EH[25]	61.30	0.40	35.00	0.55	63.64	4.93	4.06	3.33	2.75
AM-0.8-EH[25]	63.80	0.80	35.00	0.55	63.64	7.46	7.07	5.68	4.62
s3e30[4]	40.60	0.40	30.00	0.50	60.00	3.50	-	2.73	2.61
s3e45[4]	40.00	0.60	30.00	0.50	60.00	4.83	-	3.95	3.75
s4e30[4]	35.70	0.40	60.00	0.80	75.00	3.50	-	3.15	3.08
s4e45[4]	36.40	0.60	60.00	0.80	75.00	5.13	-	4.20	3.83
s5e30[4]	48.40	0.40	60.00	0.80	75.00	4.40	-	1.64	1.34
s5e45[4]	54.00	0.60	60.00	0.80	75.00	5.35	-	3.45	3.18
Beam-3A[26]	59.30	0.50	60.00	0.75	80.00	6.56	-		7.87
B403[27]	67.70	0.50	30.00	0.38	78.95	9.87	9.73	8.90	7.82
B406[27]	89.50	0.50	30.00	0.38	78.95	10.57	9.62	8.12	6.81
11(3)[28]	56.39	0.75	35.00	0.55	63.64	8.22	7.13	5.42	4.13
12(7)[28]	61.23	0.75	35.00	0.55	63.64	7.44	6.77	5.52	4.61
13(5)[28]	61.94	0.75	35.00	0.55	63.64	6.82	6.25	5.38	4.69
16(5)[28]	60.66	0.75	35.00	0.55	63.64	6.67	5.97	5.26	4.54
17(5)[28]	63.46	0.75	35.00	0.55	63.64	8.39	7.59	6.52	5.66
18(5)[28]	54.81	0.75	35.00	0.55	63.64	8.36	7.47	6.40	5.59
C25V250[29]	26.40	0.25	60.00	0.63	95.24	2.67	2.66	2.60	2.41
C35V375[29]	36.30	0.37	60.00	0.63	95.24	3.71	3.73	3.46	2.97
C45V250[29]	47.60	0.25	60.00	0.63	95.24	4.33	3.00	2.23	1.61
C45V375[29]	47.60	0.38	60.00	0.63	95.24	4.65	3.52	2.69	2.39
C45V500[29]	47.60	0.50	60.00	0.63	95.24	6.19	5.00	3.40	2.72
C20/25_Vf20[30]	27.40	0.29	65.00	1.00	65.00	2.74	2.69	2.56	2.36
C20/25_Vf45[30]	27.60	0.62	65.00	1.00	65.00	4.65	4.55	4.37	4.12
C30/37_Vf20[30]	40.90	0.28	65.00	1.00	65.00	3.61	3.57	3.50	3.31
C1B2[31]	48.60	0.50	50.00	0.75	66.67	4.47	4.55	4.58	4.40
C1B5[31]	48.60	0.50	50.00	0.75	66.67	4.30	4.30	4.17	3.86
C3B3[31]	41.40	0.50	50.00	0.75	66.67	3.82	3.82	3.67	3.45
C3B4[31]	41.40	0.50	50.00	0.75	66.67	3.80	3.87	3.78	3.58
C3B5[31]	41.40	0.50	50.00	0.75	66.67	3.84	3.69	3.44	3.16
C3B6[31]	41.40	0.50	50.00	0.75	66.67	3.90	3.90	3.90	3.82
3P-SH-60[32]	52.08	0.75	30.00	0.38	78.95	10.25	-	10.26	-
M40SF30_001[33]	40.00	0.38	60.00	0.75	80.00	3.42	3.90	3.96	3.77
M40SF30_01[33]	40.00	0.38	60.00	0.75	80.00	3.69	4.49	4.72	4.65
RC-SFRC1[34]	35.00	0.38	60.00	0.75	80.00	3.34	-	3.07	-
RC-SFRC2[34]	35.00	0.56	60.00	0.75	80.00	6.04	-	5.17	-

FIGURE 3 3D hooked-end fiber

with hooked-end type steel fibers, mostly of 3D geometry (Figure 3), presented, in general, softening behavior and with the main parameters such as concrete compressive strength, $25 < f_c < 80$ MPa, fiber volume content, $0.25\% < V_f < 0.80\%$ and fiber aspect ratio, $60 < l_f/d_f < 95$. The f_{Ri} values presented were given in the consulted papers.

3 | DISCUSSION

Assuming that the maximum experimental stresses per unit volume of fiber are expressed by Equation (6), then we can analyze the behavior of the maximum stresses for f_{R1} and f_{R3}. Note that for f_{R1}, in Figure 4, the maximum stresses are greater than the fiber yield stress, taken as the mean value from Equation (5). While for f_{R3}, in Figure 5, the maximum stress reductions are observed, with values even lower than the yield stress. These reductions are justified due to crack displacements and loss of bonding at the fiber-matrix interface. Analyzing the influences of concrete compressive strength and fiber volume on the maximum stresses, it is possible to observe a directly proportional relationship of the maximum stress with concrete compressive strength and both inversely proportional with fiber volume.

$$\sigma_{f,\max} = f_{Ri}/V_f \geq \sigma_y \tag{6}$$

The analysis of the maximum stresses from Equation (4) showed a contrary behavior to the previous observations. The maximum stresses tend to grow extremely with increasing fiber volume, Figure 6A. With values much higher than the maximum stress values from Equation (6). This is justified because Equation (6) reveals the pullout behavior of ribbed steel bars in concrete matrix with the steel fiber,[5] so the failure can occur mainly in three ways, in the concrete, in the steel, or in sliding, that is the critical stress is influenced integrally by the bond length, the concrete strength, and the sliding that in time is affected by the physical–chemical adherence of the fibers, consequently increasing the critical stress, in addition to the fibers have smaller diameters concerning the steel bars and was inversely proportional to the maximum stress, as shown in Figure 6B.

While the failure of steel fiber in the matrix occurs solely by slippage, the fiber length (l_f) is usually less than the critical length required[2] to develop the maximum tensile strength of the fiber, according to Abdallah et al.[35] increasing the embedded length of the 3D fibers did not result in an improvement on the maximum pull-out load, but increase in the total pull-out work, and also due to the loss of adhesion with the crack openings. Figure 7A reveals that the failure occurs in steel, the tensile strength of fibers influences the failure mode of the fiber that is being extracted from a concrete matrix.[19,36]
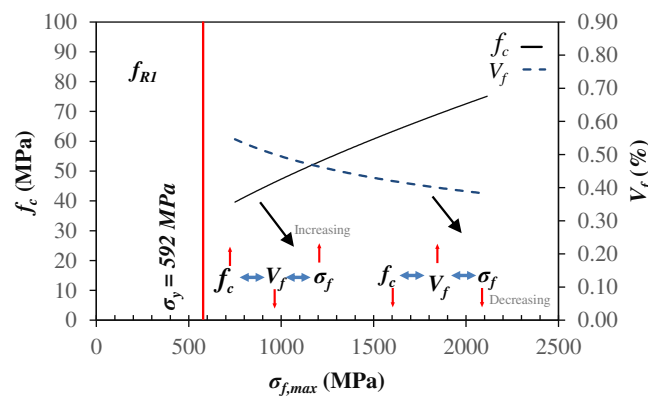

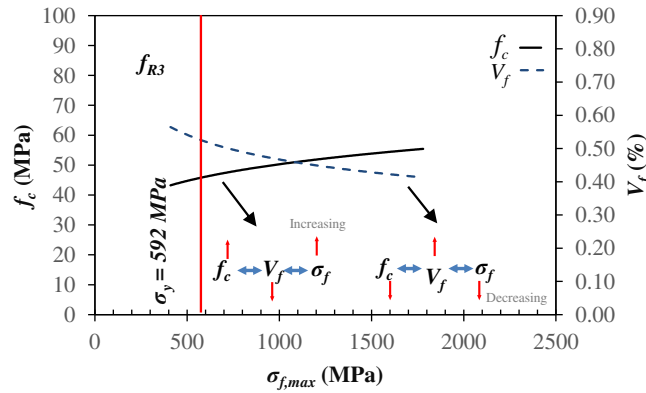**FIGURE 4** Influence of f_c and V_f on the maximum stress at f_{R1}

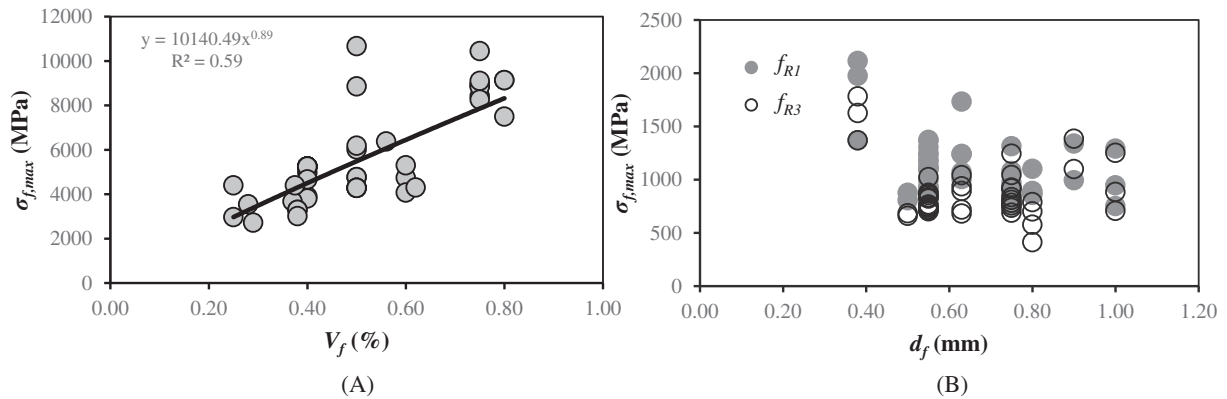**FIGURE 5** Influence of f_c and V_f on the maximum stress at f_{R3}

FIGURE 6 Influence of V_f and d_f on the maximum stress
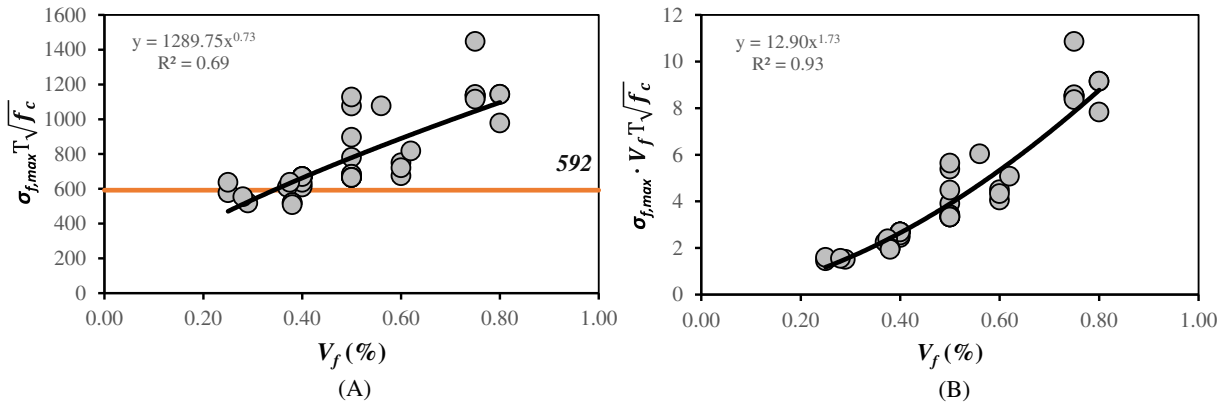

FIGURE 7 Relationship between maximum stress and fiber volume

The effect of the fiber volume reveals a difference in the order of 10^3 compared to the maximum stress (Figure 7B) of Equation (4). That is, the residual stress behavior during direct fiber pull-out is 10^3 lower than the ultimate tensile stress.

3.1 | Proposal

Thus, a new calculation model to predict residual strengths ($f_{Ri,d}$) values is proposed according to Equation (7). For the parameters for λ and φ in Equation (4), the values presented in Table 4 were used, and the maximum stress and the fiber

TABLE 4 Parameters used according to Nzambi et al[5]

V_f (%)	λ	φ
[0.00–0.39]	10	0.70[a]
[0.40–0.49]	10	0.77
[0.50–0.60]	26	0.55
[0.61–0.80]	26	0.65[a]

[a]Adopted value.

volume were also computed. Since the fiber volume is only influencing the scaling factor, it was limited to $V_f = 0.1\%$.

$$f_{Ri,d} = A \cdot \left(\sigma_{f,\max} \cdot V_f\right)^B \tag{7}$$

where, A and B are the regression coefficients.

3.1.1 | Proposed model accuracy

The mean absolute percentage error (MAPE) is a measure of how accurate a forecast system is. It measures accuracy. Compared to each observed value with their respective numerical value. The lower the MAPE values, the better the performance of the numerical model. Can be calculated by Equation (8). The MAPE is the most common measure used to forecast error and works best if there are no extremes to the data (and no zeros).

$$\text{MAPE} = \frac{1}{n} \cdot \sum_{t=1}^{n} \left| \frac{f_{Rt,Exp} - f_{Rt,d}}{f_{Rt,Exp}} \right| \cdot 100 \tag{8}$$

where:
n is the number of fitted points; $f_{Rt,\text{Exp}}$ is the experimental value; $f_{Rt,d}$ is the design value; Σ is summation notation.

3.1.2 | Residual strengths

The best-fitting coefficients (A_i, B_i) of regression analysis for f_{R1} were 1.121 and 0.91; 1.150 and 0.76 for f_{R3}. The accuracy of the predictions was satisfactory, the MAPE was approximately equal to 8% for f_{R1} and 20% for f_{R3}, within a range of variability between 15% and 25%, as shown in Figure 8. While the R^2 of f_{R1} to f_{R3} went from 92% to 54%, respectively, the same observation was verified by LAMEIRAS et al.[28]

But by analyzing the standard errors at the 95% confidence interval and comparing the experimental results with the predictions of MOD.I (from this work), MOD.II,[12] and MOD.III,[13] showing in Figure 9, it was possible to note approximation of the experimental results and with the MOD.I and MOD.III[13] models for f_{R1}. In f_{R3}, despite presenting the R^2 of 54%, the distribution followed the experimental results satisfactorily with lower standard error, while MOD.III[13] proved to be very different, presenting values for $f_{R3} > f_{R1}$. MOD.II,[12] despite presenting lower standard error, had greater dispersion and was extremely conservative. The model had the lowest coefficient of variation of only 10% and the lowest IQR of 0.15 for f_{R1}.

While for f_{R3}, all models had about the same coefficient of variation. The MOD.II[12] remained extremely conservative and MOD.III[13] proved to be extremely anti-safety, as shown in Figure 10. Figure 11 clearly shows the variability of the experimental results and the empirical models concerning the percentiles. The accuracy of the model is confirmed in both situations. Note that at f_{R3}, the model differs from the experimental results at the 89th percentile, due to the variability of some experimental f_{R3} values.

Figure 11 also highlights an approximation of MOD.III[13] with the model (MOD.I) and the experimental results, for f_{R1} and a difference in behavior from MOD.III[13] for f_{R3}, due to the model presenting high values compared to f_{R1}. Thus, an analysis of variance was performed to verify whether or not there is a statistically significant difference between the mean results of residuals strength (f_{R1} or f_{R3}), when they were compared in different models in the one-way analysis.
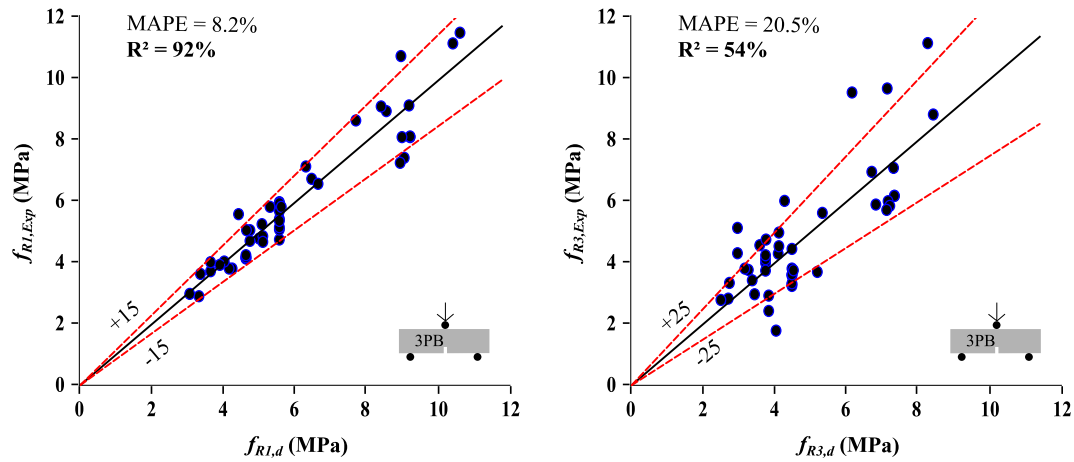
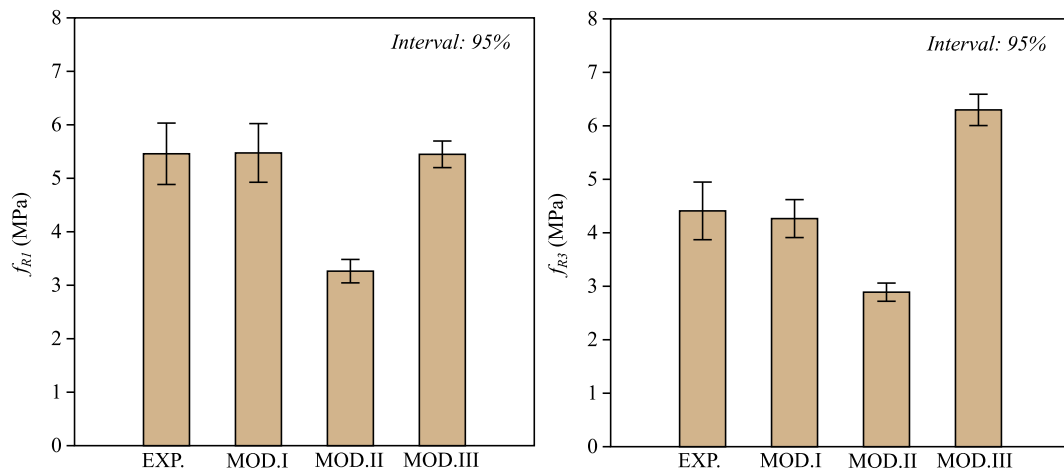**FIGURE 8** Predicted versus experimental values of the residual strengths f_{R1} and f_{R3}

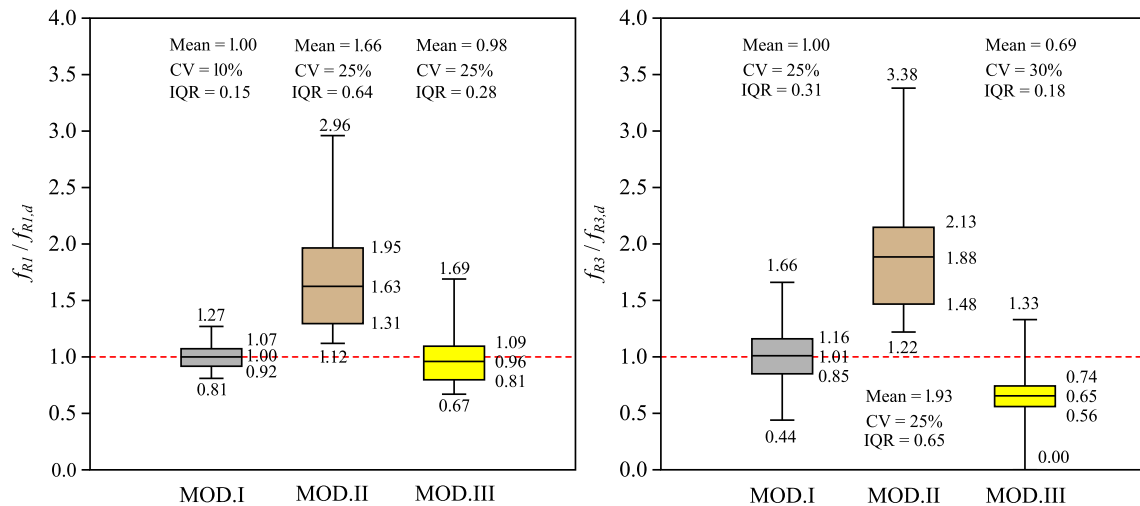**FIGURE 9** Analysis of the safety intervals with the normal distribution
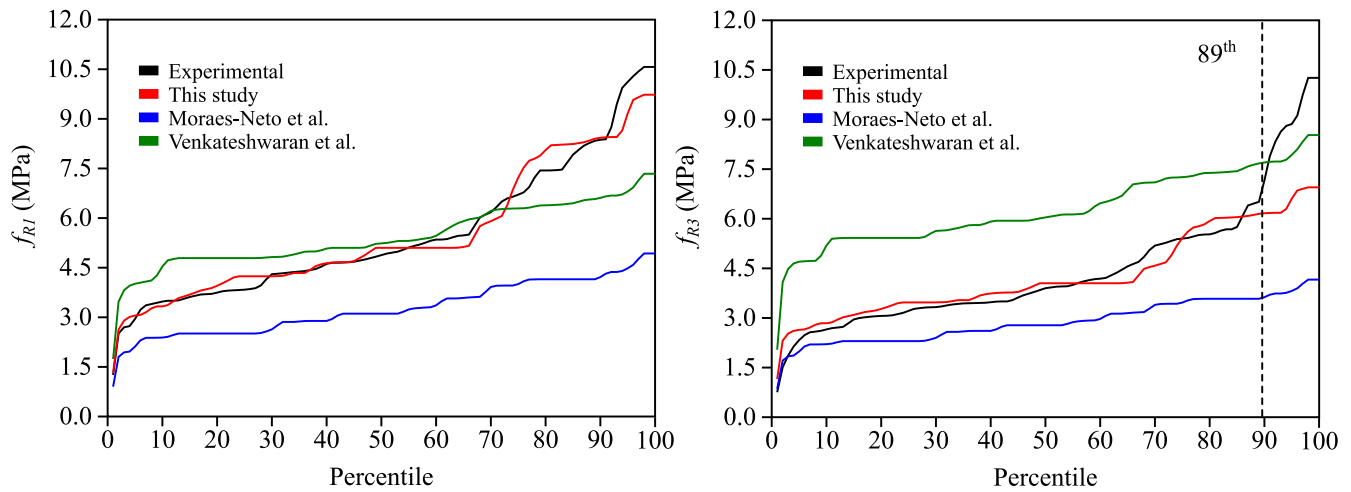

FIGURE 10 Boxplot of residual strengths

FIGURE 11   Percentile graphs of residual strengths

TABLE 5   Tukey test for f_{R1}

	Experimental	MOD.I (present study)	MOD.II[12]	MOD.III[13]
Experimental		1	**1.971E-10**	1
MOD.I (present study)	0.0713		**1.482E-10**	0.9998
MOD.II[12]	9.999	10.07		**2.373E-10**
MOD.III[13]	0.04655	0.1178	9.953	

Note: Bold values indicate that the models are not statistically equal.

TABLE 6   Tukey test for f_{R3}

	Experimental	MOD.I (present study)	MOD.II[12]	MOD.III[13]
Experimental		0.9464	**1.738E-07**	**9.106E-11**
MOD.I (present study)	0.7781		**2.194E-06**	**2.772E-12**
MOD.II[12]	8.206	7.469		0
MOD.III[13]	10.2	11.03	18.5	

Note: Bold values indicate that the models are not statistically equal.

The statistical program PAST was used and a confidence level equal to 95% and statistical significance of 5% was adopted. The results showed statistical differences between the models. Analyzing Tukey's test, presented in Tables 5 and 6, it was found that the model is statistically equal to the experimental and MOD.III,[13] for f_{R1}, in f_{R3}, the model was not statistically equal to both models, MOD.II[12] and MOD.III,[13] corroborating with the experimental results. This reveals that empirically considering only the shape factor as the only parameter for predicting the residual strengths in steel fiber concrete may provide too conservative results as shown in boxplot graphics. Besides shape factor, material properties and behavior both in compression and direct tensile tend to be closer to reality until the first crack.

Table 7 presents the summary with the remaining A and B coefficient results for f_{R2} and f_{R4}. While Table 8 presents the summary statistics of the comparisons of experimental results with the empirical models, ($f_{Ri,\text{Exp}}/f_{Ri,d}$).

TABLE 7   Summary of model results

f_{Ri}	A	B	Mean	CV (%)	MAPE (%)	R^2
f_{R1}	1.121	0.91	1.0	10.0	8.3	0.92
f_{R2}	1.170	0.83	1.0	18.0	12.5	0.77
f_{R3}	1.150	0.76	1.0	25.0	20.5	0.54
f_{R4}	1.260	0.63	1.0	31.0	25.7	0.32

TABLE 8 Summary of the statistical performance of the empirical equations for residual strength

Stat.	Proposed equations				Moraes-Neto et al.[12]			Venkateshwaran et al.[13]			
	$\dfrac{f_{R1,Exp}}{f_{R1,d}}$	$\dfrac{f_{R2,Exp}}{f_{R2,d}}$	$\dfrac{f_{R3,Exp}}{f_{R3,d}}$	$\dfrac{f_{R4,Exp}}{f_{R4,d}}$	$\dfrac{f_{R1,Exp}}{f_{R1,d}}$	$\dfrac{f_{R3,Exp}}{f_{R3,d}}$	$\dfrac{f_{R4,Exp}}{f_{R4,d}}$	$\dfrac{f_{R1,Exp}}{f_{R1,d}}$	$\dfrac{f_{R2,Exp}}{f_{R2,d}}$	$\dfrac{f_{R3,Exp}}{f_{R3,d}}$	$\dfrac{f_{R4,Exp}}{f_{R4,d}}$
AVG	1.00	1.00	1.00	1.00	1.66	1.87	1.93	0.98	0.77	0.69	0.65
SD	0.10	0.18	0.25	0.42	0.41	0.48	0.49	0.24	0.20	0.21	0.20
CV	0.10	0.18	0.25	0.31	0.25	0.25	0.26	0.25	0.26	0.30	0.31
MAPE (%)	8.3	12.5	20.5	25.7	36.5	31.5	28.5	19.6	40.4	60.5	70.6

The proposed model kept the coefficients of variation low when compared to the other two models. Also, evaluating the MAPE, it can be verified that the proposed model presented lower values too. In other words, the model guarantees an optimization in the dosage of the SFRC compared to the predictions of the other theoretical models discussed in this article.

3.1.3 | Analysis of flexural and tensile responses

According Model Code,[8] the ultimate stress of SFRC in ULS[37,38,39] is calculated by Equation (9), where, f_{Fts} represents the characteristic tensile strength in SLS and can be taken as $0.45 \cdot f_{R1}$ and takes into account the relationship between the ultimate crack opening ($w_u = 1.5$) and the $CMOD_3 = 2.5$.

$$f_{Ftu} = f_{Fts} - \frac{w_u}{CMOD_3} \cdot (f_{Fts} - 0.5 \cdot f_{R3} + 0.2 \cdot f_{R1}) \geq 0 \qquad (9)$$

Table 9 presents the residual stresses at flexure (f_{R1} and f_{R3}), the class and the classification of the material's behavior. The model proposed was satisfactory in predicting the failure mode and material behavior with the Model Code.[8] It was interesting to note the divergence of the classes of the empirical models, despite the model of Venkateshwaran et al.[13] presenting f_{R1} practically equal to the proposed model and the experimental results, the model presented a different class, 6d, and a hardening behavior, due to the high value of f_{R3} about f_{R1}. Likewise, despite the model of Moraes-Neto et al.[12] presenting a softening behavior, it also presented a different class than the experimental one. Revealing a viable optimization alternative for design with the proposed model. Another observation, the empirical regressions tend to show low variabilities of the f_{R3}/f_{R1} ratio, from 1% to 5%, while the experimental results showed variability of 22%.

Table 10 presents the comparison of residual stresses at tensile, f_{Fts} and f_{Ftu}. It is noted that the application of the residual strength proposed model presented better results, compared to the results obtained from the models References 12 and 13. The equations of Moraes-Neto et al.[12] showed that regressions with only fiber RI tends to make the model more conservative.

TABLE 9 Residual stresses at flexure and classification[6]

Author	Flexure			Classification		
	f_{R1} (MPa)	f_{R3} (MPa)	Class	f_{R3}/f_{R1}	CV	Behavior
Venkateshwaran et al.[13]	5.45	6.28	6d	1.15	0.01	Hardening
Moraes-Neto et al.[12]	3.26	2.88	3c	0.88	0.03	Softening
Proposed equations	5.47	4.26	6b	0.78	0.05	Softening
Experimental	5.46	4.41	6b	0.81	0.22	Softening

Note: Taking the average values for f_{R1} and f_{R3} from the results.

TABLE 10 Comparison of residual stresses at tensile

	Tensile			
Author	f_{Fts} (MPa)	f_{Ftu} (MPa)	$f_{Fts,Exp}/f_{Fts,d}$	$f_{Ftu,Exp}/f_{Ftu,d}$
Venkateshwaran et al.[13]	2.5	2.2	1.0	0.8
Moraes-Neto et al.[12]	1.5	1.1	1.7	1.6
Proposed equations	2.5	1.6	1.0	1.1
Experimental	2.5	1.7	-	-

Note: Taking the average values for f_{Fts} and f_{Ftu} from the results.

4 | CONCLUSIONS

The present work presented the empirical proposal for calculating the residual strengths in concrete with low steel fiber content. The model showed that it is possible to predict satisfactorily with accuracy the residual stresses of the flexural behavior from the equation of the maximum steel fiber pullout stress, with the variability of 10% and 25% for f_{R1} and f_{R3}, respectively. The model had the MAPE of 8% and 20% for f_{R1} and f_{R3}, lower values compared to other empirical models studied, and had the same material class with the experimental results, proving to be a viable alternative for pre-design[40] and dosage optimization for SFRC.

Despite presenting a low coefficient of variability and the smaller number of specimens analyzed, there is still a need for more research on the phenomenon to better understand the relationship between the variables described in this article.

PEER REVIEW
The peer review history for this article is available at https://publons.com/publon/10.1002/eng2.12490.

DATA AVAILABILITY STATEMENT
Data sharing is not applicable to this article as no new data were created or analyzed in this study.

CONFLICT OF INTEREST
The authors declare no potential conflict of interest in the manuscript.

NOTATION

A_f	nominal cross-sectional area of the fiber
A_i, B_i	proposal regression coefficients
b	beam width
d_f	fiber diameter
F	resultant force
f_c	concrete compressive strength
f_{ct}	concrete tensile strength
f_{Ft}	uniaxial first crack tensile strength of fiber reinforced concrete
f_{Fts}	residual tensile strength in the service limit state
f_{Ftu}	residual tensile strength in the ultimate limit state
F_{max}	maximum pull-out load
$f_{R,i}$	residual flexural tensile strength of fiber reinforced concrete corresponding to $CMOD_i$
$f_{Ri,d}$	design residual flexural tensile strength
$f_{Ri,Exp}$	experimental residual flexural tensile strength
H	beam height
h_{sp}	height of the prism in the notch plane
L	span
l_f	fiber length
V_f	fiber volume
λ, φ	constants of influence of the fiber on the ultimate pull-out strength[5]

σ_f	fiber tensile stress
σ_{fy}	fiber yield stress
$\sigma_{f,\max}$	maximum fiber tensile stress
τ_f	fiber bond strength
Ψ	factor which takes into account the fiber length.[13]

ORCID

Aaron Kadima Lukanu Lwa Nzambi ⬤ https://orcid.org/0000-0002-6876-271X

REFERENCES

1. Kytinou VK, Chalioris CE, Karayannis CG. Analysis of residual flexural stiffness of steel fiber-reinforced concrete beams with steel reinforcement. *Materials*. 2020;13:2698. doi:10.3390/ma13122698
2. Jain K, Singh B. Deformed steel fibres as minimum shear reinforcement — an investigation. *Structure*. 2016;7:126-137. doi:10.1016/j.istruc.2016.06.003
3. Kytinou VK, Chalioris CE, Karayannis CG, Elenas A. Effect of steel fibers on the hysteretic performance of concrete beams with steel reinforcement—tests and analysis. *Materials*. 2020;13:2923. doi:10.3390/ma13132923
4. Barros JAO. *Comportamento de betão reforçado com fibras – Análise experimental e simulação numérica*. thesis. Universidade do Porto, Faculdade de Engenharia, Portugal; 1995.
5. Nzambi AKLL, Oliveira DRC, Oliveira AM, Picanço MS. Pull-out tests of ribbed steel reinforcing bars embedded in concrete with steel fibres. *Proc Inst Civil Eng Struct Build*. 2021;174(3):181-189. doi:10.1680/jstbu.17.00180
6. Beshara FBA, Shaaban IG, Mustafa TS. Nominal flexural strength of high strength fiber reinforced concrete beams. *Arabian J Sci Eng*. 2012;37:291-300. doi:10.1007/s13369-012-0172-y
7. ACI Committee 544. Design considerations for steel fiber reinforced. American Concrete Institute, (ACI 544.4R-88). Farmington Hills (Michigan, MI); 1988. Re-approved 1999.
8. Fib Model Code. Final draft. CEB-FIP; 2013.
9. RILEM. Final recommendation TC-162-TDF: test and design methods for steel fibre reinforced concrete: σ–ε design method. *Mater Struct*. 2003;36:560-567.
10. Parmentier B, De Grove E. Dispersion of the mechanical properties of FRC investigated by different bending tests. In: Walraven JC, Stoelhorst D, eds. *Tailor Made Concrete Structures*. Taylor & Francis Group; 2008:507-512.
11. Domski J, Katzer J. Comprehensive approach to evaluation of mechanical properties of waste aggregate concrete reinforced by steel fiber. *Struct Concr*. 2020;21(1):428-436. doi:10.1002/suco.201800271
12. Moraes Neto BN, Barros JAO, Melo GSSA. A model for the prediction of the punching resistance of steel fibre reinforced concrete slabs centrically loaded. *Construct Build Mater*. 2013;46:211-223. doi:10.1016/j.conbuildmat.2013.04.034
13. Venkateshwaran A, Tan KH, Li Y. Residual flexural strengths of steel fiber reinforced concrete with multiple hooked-end fibers. *Struct Concr*. 2018;19(2):352-365. doi:10.1002/suco.201700030
14. Cardoso MG, Lameiras RM, Capuzzo VMS. Influence of concrete strength, fiber content and aspect ratio in the residual flexural strength of steel fiber reinforced self-compacting concrete. *Rev IBRACON Estrut Mater*. 2021;14(5):e14503. doi:10.1590/S1983-41952021000500003
15. Guerini V, Conforti A, Plizzari G, Kawashima S. Influence of steel and macro-synthetic fibers on concrete properties. *Fibers*. 2018;6(3):47. doi:10.3390/fib6030047
16. Yoo DY, Kim S, Kim JJ, Chun B. An experimental study on pullout and tensile behavior of ultra-high performance concrete reinforced with various steel fibers. *Construct Build Mater*. 2019;206:46-61. doi:10.1016/j.conbuildmat.2019.02.058
17. Isla F, Ruano G, Luccioni B. Analysis of steel fibers pull-out. experimental study. *Construct Build Mater*. 2015;100:183-193. doi:10.1016/j.conbuildmat.2015.09.034
18. Lee SJ, Yoo DY, Moon DY. Effects of hooked-end steel fiber geometry and volume fraction on the flexural behavior of concrete pedestrian decks. *Appl Sci*. 2019;9:1241. doi:10.3390/app9061241
19. Carrillo J, Vargas JD, Alcocer SM. Model for estimating the flexural performance of concrete reinforced with hooked end steel fibers using three-point bending tests. *Struct Concr*. 2021;22:1-24. doi:10.1002/suco.202000432
20. Dancygier A, Savir Z. Flexural behavior of HSFRC with low reinforcement ratios. *Eng Struct*. 2006;28:1503-1512. doi:10.1016/j.engstruct.2006.02.005
21. Chalioris CE, Panagiotopoulos TA. Flexural analysis of steel fibre-reinforced concrete members. *Comput Concr*. 2018;22(1):11-25. doi:10.12989/cac.2018.22.1.011
22. Choi S-W, Choi J, Lee S-C. Probabilistic analysis for strain-hardening behavior of high-performance fiber-reinforced concrete. *Concr Mater*. 2019;12(15):2399. doi:10.3390/ma12152399
23. Amin A, Foster SJ. Predicting the flexural response of steel fibre reinforced concrete prisms using a sectional model. *Cement Concr Compos*. 2016;67:1-11. doi:10.1016/j.cemconcomp.2015.12.007
24. Amin A, Foster SJ, Muttoni A. Derivation of the σ-w relationship for SFRC from prism bending tests. *Struct Concr*. 2015;16(1):93-105. doi:10.1002/suco.201400018

25. Amin A, Foster SJ. Numerical modelling of large scale steel fibre reinforcedreinforced concrete beams failing in shear. Proceedings of the ACI-Fib International Workshop Fibre Reinforced Concrete: From Design to Structural Applications; Vol. 310, 2017:161-170.

26. De Pauw P, Taerwe L, Van De Buverie N, Moerman W. Replacement of shear reinforcement by steel Fibres in Pretensioned concrete beams. In: Walraven JC, Stoelhorst D, eds. *Tailor Made Concrete Structures*. CRC Press; 2008:391-397.

27. De Wilder K, De Smedt M, Lava P, Reynders E, Vanderwalle L. Experimental analysis of the mechanical behaviour of shear-deficient pretensioned steel-fibre reinforced concrete beams. Proceedings of the 9th RILEM International Symposium on Fibre Reinforced Concrete; 2016:1248-1262.

28. Lameiras R, Barros JA, Azenha M. Influence of casting condition on the anisotropy of the fracture properties of steel fibre reinforced self-compacting concrete (SFRSCC). *Cement Concr Compos*. 2015;59:60-76. doi:10.1016/j.cemconcomp.2015.03.008

29. Lee JH. Influence of concrete strength combined with fiber content in the residual flexural strengths of fiber reinforced concrete. *Compos Struct*. 2017;168:216-225. doi:10.1016/j.compstruct.2017.01.052

30. Lourenço LAP. *Betão Reforçado com Fibras: aplicações e técnicas de inspeção reforço de elementos estruturais afetados pela ação de um fogo*. thesis. Universidade do Minho, Escola de Engenharia; 2012.

31. Oikonomou SM. *Behaviour and Design of Steel Fibre Reinforced Concrete Slabs*. thesis. Structural Engineering Research Group, Department of Civil and Environmental Engineering, Imperial College London; 2013:352.

32. Soetens T, Matthys S. Different methods to model the post-cracking behavior of hooked-end steel fbre reinforced concrete. *Constr Build Mater*. 2014;73:458-471. doi:10.1016/j.conbuildmat.2014.09.093

33. Stephen SJ, Gettu R. Rate-dependence of the tensile behaviour of fibre reinforced concrete in the quasi-static regime. *Mater Struct*. 2019;52(107):1-9. doi:10.1617/s11527-019-1405-2

34. Trindade YT. Numerical modeling of the post-cracking behavior of SFRC and its application on design of beams according to fib model code 2010. Polytechnic School of the University of São Paulo, Department of Structural and Geotechnical Engineering; 2018:171.

35. Abdallah S, Fan M, Zhou X. Pull-out behaviour of hooked end steel Fibres embedded in ultra-high performance mortar with various W/B ratios. *Int J Concr Struct Mater*. 2017;11(2):301-313. doi:10.1007/s40069-017-0193-8

36. I. Markovich, V. J. Mier and Walraven J., "Single fiber pullout from hybrid fiber reinforced concrete," *Heron*, vol. 46, no. 3, p. 191–200, 2001.

37. Narayanan R, Darwish IYS. Use of steel fibers as shear reinforcement. *ACI Struct J*. 1987;84(3):216-227.

38. Ashour SA, Hasanain GS, Wafa FF. Shear behaviour of high strength fiber reinforced concrete beams. *ACI Struct J*. 1992;89(2):176-184.

39. Swamy RN, Jones R, Chiam ATP. Influence of steel fibers on the shear resistance of lightweight concrete I-beams. *ACI Struct J*. 1993;90(1):103-114.

40. Nzambi AKLL, Oliveira DRC, Monteiro MVS, Silva LFA. Experimental analysis of steel fiber reinforced concrete beams in shear. *Rev IBRACON Estrut Mater*. 2021;15(3):e15301. doi:10.1590/S1983-41952022000300001